

# Mechanisms of multiparticle production in heavy ion collisions at high energy\*

## A. Capella

Laboratoire de Physique Théorique  
 Unité Mixte de Recherche UMR n° 8627 - CNRS  
 Université de Paris XI, Bâtiment 210, F-91405 Orsay Cedex, France

In the framework of a microscopic string model inclusive charged particle distribution and baryon and antibaryon production are described. The emphasis is put on high energies (RHIC) where shadowing corrections play a crucial role. Some recent developments on  $J/\psi$  suppression at CERN-SPS are also discussed. Possible consequences for the crucial issue of thermal equilibration of the produced system are considered.

### 1. Introduction

This work is a continuation of the one presented in ref [1], where I discussed multiparticle production at CERN-SPS energies. The present article is mainly concerned with higher energies where the effects of shadowing play a very important role. In the framework of the model presented below, the shadowing corrections can be computed from high mass diffraction practically without any new free parameter. When the effects of shadowing are taken into account, the model describes the inclusive charged particle production at RHIC as a function of centrality [2]. A comparison with the results obtained [3, 4] in the framework of the saturation model is also presented.

Another new development concerns net baryon production (stopping). It is shown that both SPS and RHIC data can be described with the same mechanism (and the same values of the parameters) used in  $pp$  interactions. This indicates that there is no evidence for an “anomalous” stopping in the heavy ion data [5].

As already observed at CERN-SPS, rare processes like strange and multistrange baryon and antibaryon production, can only be described with the

---

\* To be published in a special issue of “Acta Physica Polonica” in homage to Jan Kwiecinski

introduction of some final state interaction between the produced particles (comovers interaction) [1]. It turns out, however, that the interaction cross-sections required to describe the data are comparatively small (a few tenths of a mb) and, in view of the shortness of the interaction time (5  $\div$  7 fm) it seem quite improbable that the system can reach thermal equilibrium. In a recent development [6] reported below, we show that the same formalism of final state interaction used at CERN-SPS can describe RHIC data with the same values of the parameters. Predictions for  $\Xi$  and  $\bar{\Xi}$  production have been confirmed by recent STAR data. Predictions for  $\Omega$  and  $\bar{\Omega}$  are also given.

Finally, we analyze the new NA50 data on  $J/\psi$  suppression at CERN-SPS in the comovers approach [7] [8] and discuss expectations at RHIC.

## 2. The model

### 2.1. Hadron-Hadron Interactions

The Dual Parton Model (DPM) [9] and the Quark Gluon String Model (QGSM) [10] are closely related dynamical models of soft hadronic interactions. They are based on the large- $N$  expansion of non-perturbative QCD [11-13] and on Gribov's Reggeon Field Theory (RFT) [14]. Their main aim is to determine the mechanism of multiparticle production in hadronic and nuclear interactions. The basic mechanism is well known in  $e^+e^-$  annihilation (Fig. 1). Here the  $e^+e^-$  converts into a virtual photon, which decays into a  $q\bar{q}$  pair. In the rest system of the virtual photon the quark (with colour 3) and the antiquark (colour  $\bar{3}$ ) separate from each other producing one string (or chain) of hadrons, i.e. two back-to-back jets. Processes of this type are called one-string processes.

In hadron-hadron interactions, a one-string mechanism is also possible but only in some cases, namely when the projectile contains an antiquark (quark) of the same type than a quark (antiquark) of the target, which can annihilate with each other in their interaction. For instance in  $\pi^+p$ , the  $\bar{d}$  of  $\pi^+$  can annihilate with the  $d$  of  $p$  and a single string is stretched between the  $u$  of  $\pi^+$  (colour 3) and a diquark  $uu$  of  $p$  (colour  $\bar{3}$ ). This mechanism is also possible in  $\bar{p}p$  interactions (Fig. 2) but not in  $pp$ . This already indicates that it cannot give the dominant contribution at high energy. Indeed, when taking the square of the diagram of Fig. 2 (in the sense of unitarity) we obtain a planar graph, which is the dominant one according to the large- $N$  expansion. However, this only means that this graph has the strongest coupling. Since flavour quantum numbers are exchanged between projectile and target, this graph gives a contribution to the total cross-section that decreases as an inverse power of  $s$  ( $1/\sqrt{s}$ ). A decrease with  $s$  is always associated with flavor exchange. For instance, the charge exchange

$\pi^- p \rightarrow \pi^0 n$  cross-section also decreases as  $1/\sqrt{s}$ . Actually, the diagram in Fig. 2 corresponds to the exchange of a secondary Reggeon, with intercept close to 1/2.

In order to prevent the exchange of flavour between projectile and target, the  $\bar{d}$  and  $d$  have to stay, respectively, in the projectile and target hemispheres. Since they are coloured, they must hadronize stretching a second string of type  $\bar{d}-d$ . We obtain in this way a two-string diagram (Figs. 3-5)). Taking the square of this diagram, we obtain a graph with the topology of a cylinder (Fig. 6). It turns out that this is the simplest topology one can construct which does not vanish as  $s \rightarrow \infty$  due to flavour exchange. Therefore, we obtain in this way the dominant graph for hadron-hadron scattering at high energy. The diagram in Fig. 6 is called a Pomeron (P) and the graphs in Figs. 3-5 a cut Pomeron. Its order in the large- $N$  expansion is  $1/N^2$  [12-13]. Note that due to energy conservation the longitudinal momentum fractions taken by the two systems at the string ends have to add up to unity.

There are also higher order diagrams (in the sense of the large- $N$  expansion) with 4, 6, 8 strings which give non-vanishing contributions at high energy. An example of the next-to-leading graph for  $pp$  interactions is shown in Fig. 7. It contains four strings – the two extra strings are stretched between sea quarks and antiquarks. The square of this graph corresponds to a  $PP$  cut and has the topology of a cylinder with a handle. Its order in the large- $N$  expansion is  $1/N^4$ . The one with six strings corresponds to a  $PPP$  cut and to the topology of a cylinder with two handles (order  $1/N^6$ ), etc.

The single particle inclusive spectrum is then given by [9]

$$\begin{aligned} \frac{dN^{pp}}{dy}(y) &= \sum_n \frac{1}{\sigma_n} \sum_n \sigma_n \left( N_n^{qq-q_v}(y) + N_n^{q_v-qq}(y) + (2n-2)N_n^{q_s-\bar{q}_s}(y) \right) \\ &\simeq N_k^{qq-q_v}(y) + N_k^{q_v-qq}(y) + (2k-2)N_k^{q_s-\bar{q}_s}(y) \end{aligned} \quad (1)$$

where  $k = \sum_n n\sigma_n / \sum_n \sigma_n$  is the average number of inelastic collisions. Note that each term consists of  $2n$  strings, i.e. two strings per inelastic collisions. Two of these strings, of type  $qq-q$ , contain the diquarks of the colliding protons. All other strings are of type  $q-\bar{q}$ .

The weights  $\sigma_n$  of the different graphs, i.e. their contribution to the total cross-section, cannot be computed in the large- $N$  expansion. However, it has been shown [15] that there is a one-to-one correspondence between the various graphs in the large- $N$  expansion and those in perturbative Reggeon Field Theory [14]. We use the weights obtained from the latter – with the parameters determined from a fit to total and elastic cross-sections [9], [10]. At SPS energies we get  $k = 1.4$  and at RHIC  $k = 2$  at  $\sqrt{s} = 130$  GeV and  $k = 2.2$  at  $\sqrt{s} = 200$  GeV [2].

The hadronic spectra of the individual strings  $N(y)$  are obtained from convolutions of momentum distribution functions, giving the probability to find a given constituent (valence quark, sea quark or diquark) in the projectile or in the target, with the corresponding fragmentation functions. The dependence of  $N(y)$  on the number of collisions appears via the former. It is a result of energy conservation. (The larger the number of strings, the smaller the average invariant mass of each one).

Momentum distribution and fragmentation functions are largely determined from known Regge intercepts [9] [10]. The momentum distribution function of a valence quark in a hadron behaves as  $1/\sqrt{x}$ . As in the parton model, this behaviour results from the intercept  $1/2$  of a Reggeon trajectory. Thus, in average, the valence quark in a proton is slow and the diquark is fast due to energy conservation. Both momentum distribution and fragmentation functions are assumed to be universal, i.e. the same in all hadronic and nuclear interactions. This property gives to the model a great predictive power. Finally, individual strings are assumed to be independent. In this way, the hadronic spectra of a given graph are obtained by adding up the corresponding ones for the individual strings. This leads to a picture, in which, for any individual graph, particles are produced with only short-range (in rapidity) correlations. Long-range correlations (and a broadening of the multiplicity distributions) are due to fluctuations in the number of strings, i.e. to the superposition of different graphs with their corresponding weights. This gives a simple and successful description of the data in hadron-hadron and hadron-nucleus interactions [9] [10] [16].

## 2.2. Nucleus-Nucleus Interactions

The generalization of Eq. (1) to nucleus-nucleus collisions is rather straightforward. For simplicity let us consider the case of  $AA$  collisions and let  $n_A$  and  $n$  be the average number of participants of each nucleus and the average number of binary  $NN$  collisions, respectively. At fixed impact parameter  $b$ , we have [17]

$$\begin{aligned} \frac{dN^{AA}}{dy}(b) = & n_A(b) \left[ N_{\mu(b)}^{qq-q_v}(y) + N_{\mu(b)}^{q_v-qq}(y) + (2k-2)N_{\mu(b)}^{q_s-\bar{q}_s} \right] \\ & + (n(b) - n_A(b)) 2k N_{\mu(b)}^{q_s-\bar{q}_s}(y) \end{aligned} \quad (2)$$

$n_A(b)$  and  $n(b)$  are computed from the standard formulae in the Glauber model. The physical meaning of Eq. (2) is quite obvious. The expression in brackets corresponds to a  $NN$  collision. Since  $n_A$  nucleons of each nucleus participate in the collision, this expression has to be multiplied by  $n_A$ . Note that in Eq. (1) the average number of collisions is  $k$  – and the number

of strings  $2k$ . In the present case the total average number of collisions is  $kn$  – and the number of strings  $2kn$ . The second term in Eq. (2) is precisely needed in order to have the total number of strings required by the model. Note that there are  $2n_A$  strings involving the valence quarks and diquarks of the participating nucleons. The remaining strings are necessarily stretched between sea quarks and antiquarks. The value of  $\mu(b)$  is given by  $\mu(b) = k\nu(b)$  with  $\nu(b) = n(b)/n_A(b)$   $\mu(b)$  represents the total average number of inelastic collisions suffered by each nucleon (for more details see Section 5).

We see from eq. (2) that  $dN^{AA}/dy$  is obtained as a linear combination of the average number of participants and of binary collisions. The coefficients are determined within the model and depend on the impact parameter via  $\mu(b)$ . Note that the presence of a term proportional to the number of binary collisions is a general feature of RFT and is not related to minijet production.

As discussed in Section 2.1 the average invariant mass of a string containing a diquark at one end is larger than the one of a  $q\bar{q}$  string since the average momentum fraction taken by a diquark is larger than that of quark. It turns out that the same is true for the central plateau, i.e. :  $N^{q\bar{q}-q}(y^* \sim 0) > N^{q\bar{q}}(y^* \sim 0)$ . Let us now consider two limiting cases :

$$\text{If } N^{q_s-\bar{q}_s}(y^* \sim 0) \ll N^{q\bar{q}-q_v}(y^* \sim 0), \text{ then } \frac{dN^{AA}}{dy}(y^* \sim 0) \sim n_A \sim A^1 \quad (3)$$

$$\text{If } N^{q_s-\bar{q}_s}(y^* \sim 0) \sim N^{q\bar{q}-q_v}(y^* \sim 0), \text{ then } \frac{dN^{AA}}{dy}(y^* \sim 0) \sim n \sim A^{4/3}. \quad (4)$$

In the first case we obtain a proportionality in the number of participants  $n_A$  whereas in the second case we obtain a proportionality in the number of binary collisions. Since  $dN^{AA}/dy \equiv (1/\sigma_{AA})d\sigma^{AA}/dy$ , the latter result implies that  $d\sigma^{AA}/dy \sim A^2$ , i.e. all unitarity corrections cancel and we obtain the same result as in the impulse approximation (Born term only). This result is known as the Abramovsky-Gribov-Kancheli (AGK) cancellation and is valid for a general class of models which includes the Glauber and eikonal ones. It implies that, for the inclusive cross-section, soft and hard processes have the same  $A$ -dependence. However, the AGK cancellation is violated by diagrams related to the diffraction production of large-mass states – the so-called triple Pomeron or enhanced diagrams. These diagrams give rise to shadowing corrections as discussed below. Their effect is very important in nuclear collisions since they are enhanced by  $A^{1/3}$  factors.

### 2.3. Shadowing corrections

In Appendix A, we discuss the physical content of the AGK cutting rules and their practical realization in the probabilistic Glauber model. It is shown there that multiple scattering diagrams, resulting from the  $s$ -channel iteration of the Born term, give non-vanishing contributions to the total cross-sections (shadowing). However, in the case of the single particle inclusive cross-section, these contributions cancel identically (AGK cancellation), provided the measured particle has been produced in an inelastic interaction (cut Pomeron). If, on the contrary, the trigger particle is produced in the vertex function (blob) of the multiple scattering diagram, one obtains the same shadowing effects than in the total cross-section. This is the physical origin of the AGK violations present in DPM (see section 2.2). It is clear that if the blob has a small extension in rapidity, production from the blob will mainly contribute to the fragmentation region. Therefore, at mid-rapidities, and sufficient large energy, the AGK cancellation will be valid.

Let us consider next the contribution to the total cross-section resulting from the diffractive production of large mass states. Clearly, this is equivalent to an increase of the rapidity extension of the blob – which, in this case, can cover the mid-rapidity region. Therefore, shadowing corrections to the single particle cross-section will be present in this case, provided the measured particle is part of the diffractively produced system. As shown in Appendix A, the shadowing correction is just given by the diffractive cross-section with negative sign. (This is exactly true only for purely imaginary amplitudes). The theoretical expression of the diffractive cross-section is well-known. An important part is given by the triple-Pomeron term. It has also been measured experimentally and, thus, the shadowing corrections can be computed with no free parameters.

Considering for simplicity only the contribution of the triple Pomeron term, the effect of the shadowing corrections is obtained [18, 2] by multiplying Eq. (2) by

$$R_{AB}(b) = \frac{\int d^2s f_A(s) f_B(b-s)}{T_{AB}(b)} \quad (5)$$

where

$$f_A(b) = \frac{T_A(b)}{1 + A F(s) T_A(b)} . \quad (6)$$

Here the function  $F(s)$  is given by the integral of the ratio of the triple Pomeron cross-section  $d^2\sigma^{PPP}/dydt$  at  $t = 0$  to the single Pomeron exchange cross-section  $\sigma_p(s)$  :

$$F(s) = 4\pi \int_{y_{min}}^{y_{max}} dy \left. \frac{1}{\sigma_p(s)} \frac{d^2\sigma^{PPP}}{dy dt} \right|_{t=0} = C [\exp(\Delta y_{max}) - \exp(\Delta y_{min})] \quad (7)$$

with  $y = \ell n(s/M^2)$ , where  $M^2$  is the squared mass of the diffractive system. For a particle produced at  $y_{cm} = 0$ ,  $y_{max} = \frac{1}{2} \ell n(s/m_T)^2$  and  $y_{min} = \ell n(R_A m_N / \sqrt{3})$ .  $\Delta = \alpha_P(0) - 1 = 0.13$  and  $C$  is a constant proportional to the triple Pomeron coupling.  $R_A$  is the nuclear radius,  $T_A(b)$  the nuclear profile function and  $T_{AB}(b) = \int d^2s T_A(s) T_B(b - s)$ .

Eqs. (5) to (7) can be derived only when the triple Pomeron coupling is small and, thus, the second term in the denominator of (5) is small compared to the first one. In this case, we have  $[1 + AF(s)T_A(b)]^{-1} \sim 1 - AF(s)T_A(b)$ , and only the contribution of the triple Pomeron graph is involved in the shadowing. In general higher order rescatterings are also present. They are model dependent. The denominator in Eq. (5) correspond to the sum of all “fan” diagrams with Pomeron branchings (generalized Schwimmer model [19]).

It is interesting to study the  $A$ -dependence of the shadowing corrections in the limit of large triple Pomeron coupling (when the first term in the denominator of (6) can be neglected). In this case we find  $R_{AA} \sim A^{-2/3}$ , i.e. the  $A^{4/3}$  behaviour resulting from the AGK cancellation is reduced to  $A^{2/3}$ . This limit was considered by Kancheli many years ago [20].

Note that shadowing corrections to inclusive spectra are not especific to soft processes. The triple Pomeron terms described above are also responsible for shadowing in hard processes.

### 3. Charged Particle Multiplicities

#### 3.1. Low $p_T$

At SPS energies the limit given by Eq. (4) is not reached, and Eq. (2) leads to an  $A$  dependence of  $dN^{AA}/dy$  at  $y^* \sim 0$  in  $A^\alpha$  with  $\alpha$  only slightly above unity. ( $\alpha \sim 1.08$  between 2 and 370 participants). On the other hand, shadowing corrections are small due to phase space limitations ( $y_{max} \sim y_{min}$  in Eq. (7)). The results [2] for  $Pb$   $Pb$  collisions at  $\sqrt{s} = 17.3$  GeV are shown in Fig. 8. We see that both the absolute values and the centrality dependence are well reproduced. When the energy increases, Eq. (4) shows that the value of  $\alpha$  should increase towards  $4/3$ , in the absence of shadowing corrections. However, the effect of the latter is increasingly important and, as a result, the value of  $\alpha$  varies little with  $s$ . At  $\sqrt{s} = 130$  GeV, without shadowing corrections the  $A$ -dependence is  $A^\alpha$ , with  $\alpha \sim 1.27$  in the same range of  $n_{part}$  – a value which is not far from the maximal one,  $\alpha = 4/3$  from

Eq. (4). With the shadowing corrections the  $A$ -dependence is much weaker (lower line of the shaded area in Fig. 9) [2]. The  $A$ -dependence is now given by  $A^\alpha$  with  $\alpha \sim 1.13$  – always in the range of  $n_{part}$  from 2 to 370. As we see, the increase of  $\alpha$  from SPS to RHIC energies is rather small. This value of  $\alpha$  is predicted to change very little between RHIC and LHC, where  $\alpha \approx 1.1$ . For, the increase from  $\alpha \sim 1.27$  to  $\alpha \sim 4/3$  obtained in the absence of shadowing is compensated by an increase in the strength of the shadowing corrections, leaving the effective value of  $\alpha$  practically unchanged.

### 3.2. Large $p_T$

Let us define the ratio

$$R_{AA}(b) = \frac{d^2 N^{AA}/dy dp_T}{n(b) d^2 N^{pp}/dy dp_T} . \quad (8)$$

For central  $Au$   $Au$  collisions at  $y^* \sim 0$ , we find  $R_{AA} = A^{1.13-4/3} = 0.34$  when numerator and denominator are integrated over  $p_T$ . Clearly this value corresponds to small values of  $p_T$  which give the dominant contribution to  $dN/dy$ . This result is in agreement with the measured values of  $R_{AA}$  at  $p_T \sim < p_T >$  [21]. This was to be expected from the results presented in Fig. 9. It is interesting that these data, as well as PHENIX ones [22] show approximately the same value of  $R_{AA}$  at large  $p_T$ .<sup>1</sup>

More precisely, the data show a small increase of  $R_{AA}$  at moderate  $p_T$  and, at large  $p_T$ , they show a scaling in the number of participants – rather than in the number of binary collisions. Such a result is expected in the present approach. Indeed, at large  $p_T$  the shadowing corrections strongly decrease due to the increase of  $m_T$  in  $y_{max}$  (eq. (7)). However, the larger threshold at large  $p_T$  affects mostly the  $q\bar{q}$  strings – which have a smaller invariant mass than the  $qq$ -ones. Thus, with increasing  $p_T$  we approach the limit in eq. (3) leading to a scaling in the number of participants. The small increase of  $R_{AA}$  at moderate  $p_T$  is probably due to the Cronin effect or to a combination of this effect and jet quenching. Recently, it has been shown [23] that the Cronin effect is considerably smaller at RHIC and LHC energies than at SPS ones due to the change with energy of the coherence length.

## 4. Comparison with the saturation model

In the saturation model, the  $A$ -dependence of charged particle inclusive spectrum in the saturation regime (i.e.  $\Lambda_{QCD} \ll p_T < Q_s$ , where  $Q_s$  is the

---

<sup>1</sup> I would like to thank N. Armesto, K. Boreskov, Y. Dokshitzer, A. Kaidalov, O. Kancheli, A. Krzywicki and D. Schiff for discussions on this subject.

saturation scale) is given by [3, 4]

$$\frac{dN}{dy d^2p_T} \sim \frac{A^{2/3}}{\alpha_s(Q_s)}. \quad (9)$$

Comparison with previous section results indicates that, apart from logarithmic factors due to  $\alpha_s(Q_s)$ , we obtain the same result as in RFT with MAXIMAL shadowing. As discussed in the previous section, this result is in violent disagreement with RHIC data.

The question is then how a reasonable description of the data has been obtained in [3]. The answer is the following. The authors have considered  $dN/dy$  rather than  $dN/dy d^2p_T$ . By integrating over  $d^2p_T$  up to  $Q_s$  and assuming a  $p_T$ -broadening corresponding to  $Q_s^2 \sim A^{1/3}$  they have gained one power of  $A^{1/3}$ . Furthermore, the factor  $\alpha_s^{-1} \sim \log A^{1/3}$  increases the effective power slightly above  $A^1$  reaching agreement with experiment. The problem with this explanation is that a  $p_T$ -broadening in  $A^{1/3}$  is much larger than the one seen in the data (which is of the order of 30 % between peripheral and central collisions). In order to describe it a parametrization of the saturation scale has been introduced in [4] of the type :

$$\left[ 0.61 + 0.39 \left( \frac{n_{part}(b)}{n_{part-max}} \right)^{1/3} \right] p_{so}^2. \quad (10)$$

With this definition,  $p_{so}$  is the value of the saturation scale for the most central collisions (corresponding to  $n_{part-max} = 347$  participants). With such an expression of the saturation scale, the  $A$ -dependence of  $\frac{dN}{dy}$  is the same as that of  $dN/dy d^2p_T$  within 30 % and, with the mild  $A$ -dependence of  $\alpha_s^{-1}$  used before, it is not possible to describe the data. In view of that the authors use instead the following expression

$$\alpha_s^{-1} \sim \log \left[ \left( 0.61 + 0.39 \left( \frac{n_{part}(b)}{n_{part-max}} \right)^{1/3} \right) / \mu^2 \right] \quad (11)$$

where  $\mu^2 = \frac{\Lambda_{QCD}^2}{p_{s,0}^2}$  is chosen to be 0.6. Note the fine tuning between the 0.61 in the numerator and 0.6 in the denominator of (11). As a consequence, the value of  $\alpha_s^{-1}$  for peripheral collisions is extremely small and  $\alpha_s^{-1}$  increases by a large factor between peripheral and central collisions. With this fine tuning agreement with experiment is recovered. Note that for peripheral collisions ( $n_{part}(b) \ll n_{part-max}$ ) one is practically sitting on the Landau pole (i.e. the argument of the log is very close to unity). Note also that with  $\Lambda_{QCD} = 200$  MeV, the value of the saturation scale for the most central collisions is very small (260 MeV).

In the saturation model the  $A$ -dependence of  $dN/dy d^2p_T$  grows larger with increasing  $p_T$  and it turns out that the model can reproduce [24] the measured values of the ratio  $R_{AA}$ , Eq. (8), in the range  $1.5 \text{ GeV} < p_T < 5 \text{ GeV}$ . However, as discussed above the model has an  $A$ -dependence at lower  $p_T$  which is too weak. Thus, it is perhaps not surprising that it has the right  $A$ -dependence for larger values of  $p_T$  in some range.

The above considerations indicate that saturation is not reached at RHIC energies. The considerations in the previous section based on RFT suggest that it will not be reached at LHC either.

## 5. Nuclear Stopping Revisited

In  $pp$  collisions the net proton ( $p$ - $\bar{p}$ ) distribution is large in the fragmentation regions and has a deep minimum at mid-rapidities. In contrast to this situation a much flatter distribution has been observed [25] in central  $Pb$ - $Pb$  collisions at CERN-SPS<sup>2</sup>. In view of that, several authors have claimed that the stopping in heavy ion collisions is anomalous, in the sense that it cannot be reproduced with the same mechanism (and the same values of the parameters) used to describe the  $pp$  data. In a recent paper [5] it has been shown that this claim is not correct.

In the model described in previous sections, the net baryon can be produced directly from the fragmentation of the diquark. Another possibility is that the diquark splits producing a leading meson in the first string break-up and the net baryon is produced in a further break-up. Clearly, in the first case, the net baryon distribution will be more concentrated in the fragmentation region than in the second case. The corresponding rapidity distributions are related to the intercepts of the relevant Regge trajectories,  $\alpha_{qq}$  and  $\alpha_q$ , respectively, i.e. they are given by  $e^{\Delta y(1-\alpha)}$ . Here  $\Delta y$  is the difference between the rapidity of the produced net baryon and the maximal one. In the case of the first component, in order to slow down the net baryon it is necessary to slow down a diquark. The corresponding Regge trajectory is called baryonium and its intercept is known experimentally to be  $\alpha_{qq} = -1.5 \pm 0.5$ . For the second component, where a valence quark is slowed down, we take  $\alpha_q = 1/2$ <sup>3</sup>.

In this way we arrive to the following two component model for net baryon production out of a single nucleon

---

<sup>2</sup> Actually, a huge stopping was first observed at AGS. However, in this case we are in a different regime (intra-nuclear cascade).

<sup>3</sup> There is a third possibility in which the net-baryon transfer in rapidity takes place without valence quarks (string junction or gluonic mechanism) with intercept either  $\alpha_{S,J} = 1/2$  [26] or  $\alpha_{S,J} = 1$  [27]. We find no evidence for such a component from the existing  $pp$  and  $AA$  data. Its smallness could be related to the fact that it produces an extra string of hadrons and, thus, does not correspond to the dominant topology.

$$\begin{aligned} \frac{dN_\mu(b)}{dy}(y) = & a C_\mu Z_+^{1-\alpha_q(0)} (1 - Z_+)^{\mu(b)-3/2+n_{sq}(\alpha_\rho(0)-\alpha_\phi(0))} \\ & + (1 - a) C'_\mu Z_+^{1-\alpha_{qq}(0)} \times (1 - Z_+)^{\mu(b)-3/2+c+n_{sq}(\alpha_\rho(0)-\alpha_\phi(0))} \end{aligned} \quad (12)$$

where  $n_{sq}$  is the number of strange quarks in the hyperon  $\alpha_\rho(0) = 1/2$   $\alpha_\phi(0) = 0$ ,  $Z_+ = (e^{y-y_{max}})$ ,  $y_{max}$  is the maximal value of the baryon rapidity and  $\mu(b)$  is the average number of inelastic collisions suffered by the nucleon at fixed impact parameter  $b$  (see section 2.2). The constants  $C_\mu$  and  $C'_\mu$  are obtained from the normalization to unity of each term. The small  $Z$  behaviour is controlled by the corresponding intercept. The factor  $(1 - Z_+)^{\mu(b)-3/2}$  is obtained by requiring that the  $Z$ -fractions of all quarks at the ends of the strings, other than the one in which the baryon is produced, go to zero [9-10]. Following conventional Regge rules [28] an extra  $\alpha_\rho(0) = \alpha_\phi(0) = 1/2$  is added to the power of  $1 - Z_+$  for each strange quark in the hyperon.

The fraction,  $a$ , of the DB breaking component is treated as a free parameter. The same for the parameter  $c$  in the DP component – which has to be determined from the shape of the (non-diffractive) proton inclusive cross-section in the baryon fragmentation region. It can be seen from Eq. (12) that stopping increases with  $\mu(b)$ , i.e. with the total number of inelastic collisions suffered by each nucleon. This effect is present in the two terms of (12) and is a consequence of energy conservation. The question is whether or not this “normal” stopping is sufficient to reproduce the data. In other words whether or not the data can be described with a universal value of  $a$ , i.e. independent of  $\mu$  and the same for all reactions.

Eq. (12) gives the total net baryon density, but it does not allow to determine the relative densities of different baryon species. In order to do so we use the simple quark counting rules described in Appendix B.

A good description of the data on the rapidity distribution of  $pp \rightarrow p - \bar{p} + X$  both at  $\sqrt{s} = 17.2$  GeV and  $\sqrt{s} = 27.4$  GeV is obtained from Eq. (12) with  $a = 0.4$ ,  $c = 1$ ,  $\alpha_q = 1/2$  and  $\alpha_{qq} = -1$ . The results are shown in Table 1 at three different energies, and compared with the data. As we see the agreement is reasonable. For comparison with the nucleus-nucleus results, all values in Table 1 have been scaled by the number of participants pairs in central  $Pb Pb$  and  $Au Au$  collisions ( $n_A = 175$ ). As it is well known, a pronounced minimum is present at  $y^* = 0$ . There is also a substantial decrease of the mid-rapidity yields with increasing energy. Also, the mid-rapidity distributions get flatter with increasing energy since the net proton peaks are shifted towards the fragmentation regions.

It is now possible to compute the corresponding net baryon production

in heavy ion collisions and to check whether or not the data can be described with Eq. (12) using the same set of parameters as in  $pp$ .

The results [5] for net proton ( $p - \bar{p}$ ) and net baryon ( $B - \bar{B}$ ) production in central  $Pb Pb$  collisions at  $\sqrt{s} = 17.2$  GeV and central  $Au Au$  collisions at  $\sqrt{s} = 130$  GeV are given in Table 2. The centrality is defined by the average number of participants –  $n_{part} = 2n_A = 350$  in both cases. Experimental results are given in brackets.

The comparison of column 2 with the  $pp$  results in Table 1 at the same energy, shows the well known change in the shape of the rapidity distribution between  $pp$  and central  $Pb Pb$  collisions at SPS. The minimum at  $y^* = 0$  is much less pronounced in  $Pb Pb$  and the net proton peaks in the  $pp$  fragmentation regions are shifted to  $y^* \sim \pm 1.5$ . More interesting are the results in columns 4 and 5 which contain the predictions for  $Au Au$  at RHIC. We see that the shape of the rapidity distribution is very different from the one at SPS.

In conclusion, we have found that “anomalous” stopping is not needed in order to describe the present data. Related models have been proposed in [29-31]. The results for heavy ion collisions are rather similar to the ones obtained from eq. (12). However, in these models there is some increase in the size of the second component with the number of inelastic collisions, i.e. some anomalous stopping is present.

## 6. Hyperon-Antihyperon Production

Strange particle production and, in particular, of multistrange hyperons has been proposed as a signal of Quark Gluon Plasma formation. Flavor equilibration is very efficient in a plasma due to large gluon densities and low thresholds. An analysis of the results at SPS in the framework of the present model has been presented in [31]. In the following we concentrate on RHIC results.

A general result in DPM is that the ratios  $B/h^-$  and  $\bar{B}/h^-$  of baryon and antibaryon yields over negatives decrease with increasing centralities. This is easy to see from Eq. (2). The production from  $q_s - \bar{q}_s$  strings scales with the number of binary collisions. These strings have a smaller (average) invariant mass than the  $qq-q$  strings and, thus, are more affected by the thresholds needed for  $B\bar{B}$  pair production. As a consequence, the centrality dependence of  $B$  and  $\bar{B}$  production will be smaller than the one of negatives. (The same effect was discussed in Section 3.2 in connection with large  $p_T$  production). The effect is rather small at RHIC energies. However, it is sizable and increases with the mass of the produced baryon. In contrast with this situation, the data for  $\Lambda$ 's show no such decrease and an increase is present for  $\Xi$  production. Data on  $\Omega$  production are not yet

available. However, SPS data clearly show a hierarchy in the sense that the enhancement of baryon production increase with the mass (or strange quark content) of the produced baryon.

The only way out we have found is to give up the assumption of string independence. Until now we have assumed that particles produced in different strings are independent from each other. In the following we allow for some final state interactions between comoving hadrons or partons (see Section 8). We proceed as follows.

The hadronic densities obtained in Section 2 are used as initial conditions in the gain and loss differential equations which govern final state interactions. In the conventional derivation [32] of these equations, one uses cylindrical space-time variables and assumes boost invariance. Furthermore, one assumes that the dilution in time of the densities is only due to longitudinal motion<sup>4</sup>, which leads to a  $\tau^{-1}$  dependence on the longitudinal proper time  $\tau$ . These equations can be written [32] [31]

$$\tau \frac{d\rho_i}{d\tau} = \sum_{k\ell} \sigma_{k\ell} \rho_k \rho_\ell - \sum_k \sigma_{ik} \rho_i \rho_k. \quad (13)$$

The first term in the r.h.s. of (13) describes the production (gain) of particles of type  $i$  resulting from the interaction of particles  $k$  and  $\ell$ . The second term describes the loss of particles of type  $i$  due to its interactions with particles of type  $k$ . In Eq. (13)  $\rho_i = dN_i/dy d^2s(y, b)$  are the particles yields per unit rapidity and per unit of transverse area, at fixed impact parameter. They can be obtained from the rapidity densities (2) using the geometry, i.e. the  $s$ -dependence of  $n_A$  and  $n$ . The procedure is explained in detail in [7] where the pion fragmentation functions are also given. Those of kaons and baryons can be found in [6].  $\sigma_{k\ell}$  are the corresponding cross-sections averaged over the momentum distribution of the colliding particles.

Equations (13) have to be integrated from initial time  $\tau_0$  to freeze-out time  $\tau_f$ . They are invariant under the change  $\tau \rightarrow c\tau$  and, thus, the result depends only on the ratio  $\tau_f/\tau_0$ . We use the inverse proportionality between proper time and densities and put  $\tau_f/\tau_0 = (dN/dy d^2s(b))/\rho_f$ . Here the numerator is given by the DPM particles densities. We take  $\rho_f = [3/\pi R_p^2](dN^-/dy)_{y^* \sim 0} = 2 \text{ fm}^{-2}$ , which corresponds to the density of charged and neutrals per unit rapidity in a  $pp$  collisions at  $\sqrt{s} = 130 \text{ GeV}$ . This density is about 70 % larger than at SPS energies. Since the corresponding increase in the  $AA$  density is comparable, the average duration

---

<sup>4</sup> Transverse expansion is neglected. The fact that HBT radii are similar at SPS and RHIC and of the order of magnitude of the nuclear radii, seems to indicate that this expansion is not large. The effect of a small transverse expansion can presumably be taken into account by a small change of the final state interactions cross-sections.

time of the interaction will be approximately the same at CERN SPS and RHIC – about 5 to 7 fm.

Next, we specify the channels that have been taken into account in our calculations. They are

$$\pi N \rightleftarrows K\Lambda(\Sigma), \quad \pi\Lambda(\Sigma) \rightleftarrows K\Xi, \quad \pi\Xi \rightleftarrows K\Omega \quad (14)$$

We have also taken into account the strangeness exchange reactions

$$\pi\Lambda(\Sigma) \rightleftarrows KN, \quad \pi\Xi \rightleftarrows K\Lambda(\Sigma), \quad \pi\Omega \rightleftarrows K\Xi \quad (15)$$

as well as the channels corresponding to (14) and (15) for antiparticles<sup>5</sup>. We have taken  $\sigma_{ik} = \sigma = 0.2$  mb, i.e. a single value for all reactions in (14) and (15) – the same value used in ref. [31] to describe the CERN SPS data.

Before discussing the numerical results and the comparison with experiment let us examine the qualitative effects of comovers interaction. As explained in the beginning of this Section, without final state interactions all ratios  $K/h^-$ ,  $B/h^-$  and  $\bar{B}/h^-$  decrease with increasing centrality. The final state interactions (14), (15) lead to a gain of strange particle yields. The reason for this is the following. In the first direct reaction (14) we have  $\rho_\pi > \rho_K, \rho_N > \rho_\Lambda, \rho_\pi \rho_N \gg \rho_K \rho_\Lambda$ . The same is true for all direct reaction (14). In view of that, the effect of the inverse reactions (14) is small. On the contrary, in all reactions (15), the product of densities in the initial and final state are comparable and the direct and inverse reactions tend to compensate with each other. Baryons with the largest strange quark content, which find themselves at the end of the chain of direct reactions (14) and have the smallest yield before final state interaction, have the largest enhancement. Moreover, the gain in the yield of strange baryons is larger than the one of antibaryons since  $\rho_B > \rho_{\bar{B}}$ . Furthermore, the enhancement of all baryon species increases with centrality, since the gain, resulting from the first term in Eq. (13), contains a product of densities and thus, increases quadratically with increasing centrality.

### 6.1. Numerical Results

All our results refer to mid-rapidities. The calculations have been performed in the interval  $-0.35 < y^* < 0.35$ . In Fig. 10a-10d we show the ra-

---

<sup>5</sup> To be precise, of all possible charge combinations in reactions (14), we have only kept those involving the annihilation of a light  $q\bar{q}$  pair and production of an  $s\bar{s}$  in the  $s$ -channel. The other reactions, involving three quarks in the  $t$ -channel intermediate state, have substantially smaller cross-sections and have been neglected. All channels involving  $\pi^0$  have been taken with cross-section  $\sigma/2$  since only one of the  $u\bar{u}$  and  $d\bar{d}$  components of  $\pi^0$  can participate to a given charge combination. For details see the first paper of [31].

pidity densities of  $B$ ,  $\overline{B}$  and  $B - \overline{B}$ <sup>6</sup> versus  $h^- = dN^-/d\eta = (1/1.17)dN/dy$  and compare them with available data [33-35]. We would like to stress that the results for  $\Xi$  and  $\overline{\Xi}$  were given [6] before the data [35]. This is an important success of our approach.

In first approximation, the yields of  $p$ ,  $\overline{p}$ ,  $\Lambda$  and  $\overline{\Lambda}$  yields over  $h^-$  are independent of centrality. Quantitatively, there is a slight decrease with centrality of  $p/h^-$  and  $\overline{p}/h^-$  ratios, a slight increase of  $\Lambda/h^-$  and  $\overline{\Lambda}/h^-$  and a much larger increase for  $\Xi$  ( $\overline{\Xi}$ )/ $h^-$  and  $\Omega$  ( $\overline{\Omega}$ )/ $h^-$ . This is better seen in Fig. 11a and 11b where we plot the yields of  $B$  and  $\overline{B}$  per participant normalized to the same ratio for peripheral collisions versus  $n_{part}$ . The enhancement of  $B$  and  $\overline{B}$  increases with the number of strange quarks in the baryon. This increase is comparable to the one found at SPS between  $pA$  and central  $Pb$   $Pb$  collisions, especially for antibaryons. The ratio  $K^-/\pi^-$  increases by 30 % in the same centrality range, between 0.11 and 0.14 in agreement with present data. The ratios  $\overline{B}/B$  have a mild decrease with centrality of about 15 % for all baryon species – which is also seen in the data. Our values for  $N^{ch}/N_{max}^{ch} = 1/2$  are :  $\overline{p}/p = 0.69$ ,  $\overline{\Lambda}/\Lambda = 0.74$ ,  $\Xi/\overline{\Xi} = 0.79$ ,  $\Omega/\overline{\Omega} = .83$ , to be compared with the measured values [36] :

$$\overline{p}/p = 0.63 \pm 0.02 \pm 0.06 \quad , \quad \overline{\Lambda}/\Lambda = 0.73 \pm 0.03 \quad , \quad \Xi/\overline{\Xi} = 0.83 \pm 0.03 \pm 0.05 \, .$$

The ratio  $K^+/K^- = 1.1$  and has a mild increase with centrality, a feature also seen in the data.

Note that a single parameter has been adjusted in order to determine the absolute yields of  $B\overline{B}$  pair production, namely the  $\overline{p}$  one – which has been adjusted to the experimental  $\overline{p}$  value for peripheral collisions. The yields of all other  $B\overline{B}$  pairs has been determined using the quark counting rules given in Appendix B. The experimental data in Fig. 10 are not corrected for feed-down from weak decays. If these corrections were the same (in percentage) for all baryon species, our results should be compared with uncorrected yields. This seems to be the case for  $p$ ,  $\overline{p}$ ,  $\Lambda$  and  $\overline{\Lambda}$  where the feed-down corrections are of the order of 20 %. As a consequence, our predictions for  $\Xi$ ,  $\overline{\Xi}$ ,  $\Omega$  and  $\overline{\Omega}$  have a 20 % uncertainty.

Although the inverse slopes (“temperature”) have not been discussed here, let us note that in DPM they are approximately the same for all baryons and antibaryons both before and after final state interaction – the effect of final state interaction on these slopes being rather small [37].

---

<sup>6</sup> In the numerical calculations the net baryon yields have been obtained using the approach in [6] and [31]. This approach is conceptually different from the one in Section 5 but the numerical results are similar.

## 7. New $J/\psi$ suppression data and the comovers interpretation

The NA38-NA50 collaboration have observed a decrease of the ratio of  $J/\psi$  to dimuon (DY) cross-sections with increasing centrality in  $SU$  and  $Pb Pb$  collisions. The same phenomenon has been observed in  $pA$  collisions with increasing values of  $A$ . In this case, it is interpreted as due to the interaction of the pre-resonant  $c\bar{c}$  pair with the nucleons of the nucleus it meets in its path (nuclear absorption). As a result of this interaction, the  $c\bar{c}$  pair is modified in such a way that, after interaction, it has no projection into  $J/\psi$  (a  $D\bar{D}$  pair is produced instead). The  $J/\psi$  survival probability  $S_{abs}$  is well known (see for instance eq. (7) of [7]) and depends on a single free parameter  $\sigma_{abs}$ , i.e. the absorptive  $c\bar{c} - N$  cross section.

The NA50 collaboration has shown that the  $J/\psi$  suppression in  $Pb Pb$  collisions has an anomalous component, i.e. it cannot be reproduced using nuclear absorption alone. Two main interpretations have been proposed : deconfinement and comovers interaction. The latter mechanism has been described in Section 6 for strange particle production. In the case of  $J/\psi$  suppression, a single channel is important namely  $c\bar{c}$  (or  $J/\psi$ ) interacting with comoving hadrons and producing a  $D\bar{D}$  pair. In this case, eq. (13) can be solved analytically. The expression of the survival probability  $S_{co}$  can be found in [7] (see eq. (8)). It depends on a free parameter  $\sigma_{co}$ , i.e. the effective cross-section for the comovers interaction.

Two important sets of new data have been presented recently by the NA50 collaboration on  $pA$  [38] and  $Pb Pb$  collisions [39]. Before these data were available, the NA50 interpretation of the data was as follows. The  $pA$ ,  $SU$  and peripheral  $Pb Pb$  data can be described with nuclear absorption alone, with  $\sigma_{abs} = 6.4 \pm 0.8$  mb. At  $E_T \sim 40$  GeV there is a sudden onset of anomalous suppression with a steady fall off at large  $E_T$ . However, at variance with this view, the most peripheral  $Pb Pb$  points lied above the nuclear absorption curve – which extrapolates  $pA$  and  $SU$  data.

The new  $pA$  data indicate a substantially smaller value of the absorptive cross-section. However, within errors,  $pA$  and  $SU$  data can still be described with  $\sigma_{abs} = 4.4 \pm 0.5$  mb [38]. The new  $Pb Pb$  preliminary data, taken in 2000 with a target under vacuum, are consistent with previous ones except for the most peripheral ones – which are now lower and consistent with the nuclear absorption curve [39]. In this way, the NA50 interpretation remains valid. However, the new data lend support to the interpretation based on comovers interaction. Indeed, due to the smaller value of  $\sigma_{abs}$  there is more room for comovers interaction (i.e. for anomalous suppression) in  $SU$ .

Actually, before the new data were available, it has been argued [8] that a value of  $\sigma_{abs} = 4.5$  mb is also consistent within errors with the old  $pA$  data. Using this value and  $\sigma_{co} = 1$  mb it has been possible to describe all available

data within the comovers scenario [7, 8, 40]. There was, however, a caveat, as pointed out in [8]. Indeed, there was a mismatch of about 30 % between the absolute normalizations in *SU* and *Pb Pb*. Actually, the ratio of the first normalization to the second one is only  $1.04 \pm 0.02$  [38]. (This factor takes into account both the isospin correction in *SU* and the rescaling in energy). This mismatch was induced by the high values of the most peripheral *Pb Pb* data in the old NA50 data. Indeed, since the relative contribution of the comovers to  $J/\psi$  suppression is larger for central collisions, the centrality dependence of the  $J/\psi$  suppression gets flatter (steeper) with decreasing (increasing) values of  $\sigma_{co}$  (at fixed  $\sigma_{abs}$ ). In order to reproduce the shape of the  $J/\psi$  over *DY* ratio, from very peripheral to central collisions, in the old NA50 analysis, a value of  $\sigma_{co} = 1$  mb was required. On the other hand the new data are described with a smaller value  $\sigma_{co} = 0.65$  mb. This decrease of  $\sigma_{co}$  leads to a decrease of the absolute normalization, which is now consistent with the *SU* one<sup>7</sup>.

The results [42] of the comover interaction model with  $\sigma_{abs} = 4.5$  mb and  $\sigma_{co} = 0.65$  mb are presented in Fig. 12. As in ref. [40] the steady fall-off of the  $J/\psi$  over *DY* ratio at large  $E_T$  is obtained introducing the  $E_T$  fluctuations. The agreement with the new NA50 data [39] is quite satisfactory. The absolute normalization is 47. The corresponding one in *SU* is 45 in perfect agreement with the expectations discussed above.

It is interesting to note that the data obtained using the  $E_T$  calorimeter and the zero-degree calorimeter (ZDC) analysis are consistent with each other when using the measured  $E_T - EZDC$  correlation. This result was predicted in ref. [8].

Next, I would like to discuss briefly the expectations for  $J/\psi$  suppression at RHIC in the comovers interaction model. The calculation of the survival probability  $S_{co}$  is quite safe. Indeed, since  $\sigma_{co}$  is a cross-section near threshold, the same value obtained at SPS should be used at RHIC. The situation is quite different for  $S_{abs}$ . Many authors assume that  $\sigma_{abs}$  is the same at RHIC and at SPS. It has also been suggested that it can be significantly larger at RHIC. However, it seems plausible that at mid-rapidities, nuclear absorption at RHIC is small due to the fact that, contrary to SPS, the  $c\bar{c}$  pair is produced outside the colliding nuclei. It is therefore crucial to have data on  $J/\psi$  production in  $pA$  interactions at RHIC. If  $S_{abs} \sim 1$  the  $J/\psi$  suppression at RHIC and SPS will be comparable since the smallness of the nuclear absorption will be approximately compensated by the increase of the comovers suppression – due to a larger comovers density at RHIC. Very

---

<sup>7</sup> It is interesting that almost the same value of  $\sigma_{co}$  ( $\sigma_{co} = 0.7$  mb) was obtained in [41] from an analysis of *SU* data and old *Pb Pb* data (which covered a much smaller centrality range). In [41] the absolute normalization in *SU* and *Pb Pb* were in good agreement with each other.

preliminary data tend to indicate that this is indeed the case.

A quantitative analysis of the new NA50 data in the deconfining scenario is still missing. On the other hand, the centrality dependence of the average  $p_T$  of  $J/\psi$  is better described in the comovers approach than in a deconfining scenario [43]. At RHIC energies, a small nuclear absorption in  $pA$  collisions (i.e.  $S_{abs} \sim 1$ ), would be a very interesting situation in order to discriminate the comovers interaction model from a deconfining scenario. Indeed, in the latter, the shape of the centrality dependence would be almost flat for peripheral collisions (below the deconfining threshold) and would decrease above the threshold. Such a behaviour would be a clear signal of deconfinement. On the contrary, in the comovers scenario, the fall-off would be continuous, from peripheral to central collisions, and determined by the same value of  $\sigma_{co}$  obtained from CERN SPS data.

## 8. Conclusions

Quark Gluon Plasma (QGP) formation is obtained in statistical QCD, i.e. QCD applied to a system in thermal equilibrium. Therefore, one of the main issues in heavy ions physics is to determine whether or not the produced final state reaches thermal equilibrium. An argument in favor of equilibrium is the fact that particle abundances are well described in terms of statistical models. However, one should take into account that statistical models are also very successful in  $pp$  and even  $e^+e^-$  interactions. Therefore, it is important to study whether or not particle abundances can be obtained in a microscopic model such as DPM.

As a starting point we have assumed that particles produced in different strings are independent (see Section 2). In this case thermal equilibrium cannot be reached no matter how large the energy density is. Indeed, in this case a large energy-density is the result of piling up a large number of independent strings. The assumption of independence of strings works remarkably well in  $hh$  and  $hA$  interactions [9] [10] – even in the case of event samples with 5 or 6 times the average multiplicity – indicating that no sizable final state interaction is present in these reactions. In nucleus-nucleus collisions, we have described charged particle inclusive production and its centrality dependence. The model exhibits a term proportional to the number of binary collisions – which has been seen in the data both at SPS and RHIC. The presence of such a term is required by unitarity and is not due to minijets.

However, it is clear that in heavy ion collisions, where several strings occupy a transverse area of  $1 \text{ fm}^2$ , the assumption of string independence has to break down. This is indeed the case. As we have seen, some data cannot be described without final state interaction. It could have happened

that this final state interaction is so strong that the string picture breaks down and becomes totally useless. This does not seem to be the case. On the contrary, present data can be described using the particle densities computed in the model as initial conditions in the gain and loss (transport) equations governing the final state interaction. The interaction cross-section turns out to be small (of the order of a few tenths of a mb). Due to this smallness and to the limited interaction time available, final state interaction has an important effect only on rare processes, in particular  $\Xi$ ,  $\Omega$  and  $J/\psi$  production. The bulk of the final state is not affected.

Of course it is not possible to conclude that thermal equilibrium has not reached. However, particle abundances not only do not allow to conclude that it has been reached, but, on the contrary, their centrality dependence tends to indicate that this is not the case. Let us consider for instance  $p$  and  $\bar{p}$  production. In our model, their yields are practically not affected by final state interaction, i.e. they are practically the same assuming string independence. Yet, the model reproduces the data, from very peripheral to very central interaction. This success would be difficult to understand in a QGP scenario in which for peripheral collisions (below the critical density) there is strong, non-equilibrated,  $p\bar{p}$  annihilation, which becomes equilibrated for central ones, above the critical density. More generally, the QGP scenario would be strongly supported if some kind of threshold would be found in the strange baryon yields around the critical density value. At SPS energies, evidence for such a threshold in the  $\bar{\Xi}$  yield has been claimed by the NA57 collaboration [44]. Unfortunately, these data only cover a limited range of centrality. In contrast to this situation the RHIC data explore the whole centrality range from very peripheral to very central collisions and the centrality dependence of the yields of  $p$ ,  $\Lambda$ ,  $\Xi$  and their antiparticles shows no structure whatsoever. If the same happens for  $\Omega$  and  $\bar{\Omega}$  production (as predicted in our approach) the case for QGP formation from strange baryon enhancement will be rather weak.

Finally, it should be stressed that the final state interaction of comovers in our approach is by no means a trivial hadronic effect. Indeed, the interaction of comovers starts at the early times where densities, as computed in DPM, are very large. In this situation the comovers are not hadrons (there are several of them in the volume occupied by one hadron, and, moreover, at these early times hadrons are not yet formed). This is probably the reason why in our approach the comover interaction cross-sections required to describe the data are smaller than in a hadron gas model.

Before concluding, I would like to say that it is an honor and a pleasure to contribute to this special issue of *Acta Physica Polonica* in hommage to my friend Jan Kwiecinski. I would also like to acknowledge his important contributions to the model presented here, realized during his (too rare)

visits to Orsay. In particular he played an important role in the generalization of the Dual Parton Model to heavy ions collisions [17] and also in introducing [45] a semi-hard component in the model.

## Appendix A

### *a) Reggeon Field Theory versus Glauber Model*

The reggeon calculus or reggeon field theory (RFT) [14] provides a field theoretical formulation of the eikonal (for  $hh$  collisions) or the Glauber (for  $hA$  and  $AB$ ) models, valid at high energies. The main difference between the RFT and the Glauber model is that, at high energies, the coherence length is large and the whole nucleus is involved in the interaction. Moreover, due to the space-time development of the interaction, when, at high energy a projectile interacts inelastically with a nucleon of the nucleus, the formation time of (most of) the produced particles is larger than the nuclear size and, thus, particles are produced outside the nucleus. Therefore, planar diagrams give a vanishing contribution at high energy. The relevant diagrams are non-planar, describing the “parallel” interactions of constituents of the projectile with the target nucleons (in the case of an  $hA$  collision). This picture is in clear contrast with the Glauber model, in which the projectile undergoes successive (billiard ball type of) collisions with the nucleons of the target.

In spite of these differences, one recovers the Glauber formula in first approximation. This formula corresponds to the contribution of the initial state (on-shell projectile pole) to the various rescattering terms. In RFT one has, besides these contributions, also the contributions due to low mass and high mass diffractive excitations of the projectile. The latter are very important since, as we have seen in Section 2.3, they give rise to shadowing corrections.

### *b) Cutting Rules*

An important feature of RFT is that it obeys to the so-called AGK cutting rules [46]. These rules allow to relate to each other the different  $s$ -channel discontinuities of a given graph, and also to relate them to the contribution of this graph to the total cross-section. In this way, they provide a powerful link between total cross-section and multiparticle production. In order to illustrate these rules, let us consider the case of an interaction of a hadron  $h$  with two different nucleons of the target nucleus  $A$  (with  $A - 2$  spectators), and let us assume that the object exchanged in the  $t$ -channel

of each collision is purely imaginary (Pomeron).

Let us consider the cutting by a plane in between the two interactions (i.e. in between the two Pomerons). We obtain in this way a diffractive intermediate state containing a large rapidity gap. Let us call +1 its contribution to  $\sigma_{tot}$ . From the cutting rules we find that the inelastic contribution obtained cutting through one of the interactions (an interference term) has a weight  $-2$  relative to the previous one. Since there are two interactions one can cut through, one obtains  $-4$ . Finally, cutting by a plane through the two interactions (which is possible since the graph is non-planar) has a relative weight  $+2$ . This last contribution is also inelastic and has an average multiplicity which is twice that of the previous one. The total contribution of this double scattering, to  $\sigma_{tot}$  is thus equal to  $+1 - 4 + 2 = -1$ , a negative contribution. The total contribution to the non-diffractive inelastic cross-section is  $\sigma_{ND} = -4 + 2 = -2$ . We see in this way that the (negative) contribution of a double interaction to  $\sigma_{ND}$  is two times larger, in absolute value than its contribution to  $\sigma_{tot}$ . In the case of  $n$  collisions the corresponding factor is  $2^n$ .

Let us now consider the contribution of a double interaction to the non-diffractive single particle inclusive cross-section  $d\sigma/dy$ . This contribution is  $-4 + 2 \times 2 = 0$ . Indeed, in the case of the cut through the two interactions the contribution to  $d\sigma/dy$  has an extra factor 2 since the triggered particle can be produced in either of the two interactions. It turns out that such a cancellation is true to all orders in the number of interactions. We obtain in this way the so-called AGK cancellation. All rescattering corrections of the Glauber type cancel identically in  $d\sigma/dy$ . Only the term with a single interaction is left – which is proportional to  $A^1$  in  $pA$  interactions.

Note that the crucial ingredient in obtaining the AGK cancellation is the fact that the triggered particle has been produced in a cut interaction – which gives the extra factor 2 for two cut interactions. The other possibility is that, the trigger particle is emitted from the (cut) vertex function (blob). Clearly, in this case the extra factor 2 is absent and the AGK cancellation is not valid. In this case the shadowing corrections are the same as in the total cross-section.

The AGK cutting rule described above are quite general. They are valid in any field theory in which the vertex functions obey the general properties of unitarity, crossing and large  $p_T$  damping. The Glauber model is a particular example in which the AGK rules are valid. Their derivation in this case is straightforward, as discussed below.

### *c) The Probabilistic Glauber Model and the Cutting Rules*

Let us consider for simplicity  $pA$  scattering. The main formula of the

probabilistic Glauber model is the one that gives the cross-section  $\sigma_n$  for  $n$  inelastic collisions of the projectile with  $n$  nucleons of the target nucleus, at fixed impact parameter  $b$  :

$$\sigma_n(b) = \binom{A}{n} (\sigma_{inel} T_A(b))^n (1 - \sigma_{inel} T_A(b))^{A-n} \quad (\text{A.1})$$

where  $\sigma_{inel}$  is the proton-nucleon inelastic cross-section and  $T_A(b)$  is the nuclear profile function. This equation is just the Bernoulli's formula for composite probabilities. The first factor is a trivial combinatorial factor corresponding to the different ways of choosing  $n$  nucleons out of  $A$ . The second one gives the probability of having  $n$  inelastic  $pN$  collisions at given  $b$ . The third one is the probability that the remaining  $A - n$  nucleons do not interact inelastically. Let us consider first a term with two collisions both of which are inelastic. The corresponding cross-section is  $\sigma_2^2(b) = \binom{A}{2} (\sigma_{inel} T_A(b))^2$  i.e. a positive term. Let us now consider the case of two collisions only one of which is inelastic. The corresponding (interference) term is  $\sigma_2^1(b)$  obtained from eq. (A.1) by putting  $n = 1$  and taking the second term in the expansion of the last factor. We get  $\sigma_2^1(b) = -A(A - 1)(\sigma_{inel} T_A(b))^2$ . We see that  $\sigma_2^1(b) = -2\sigma_2^2(b)$ . Thus, a rescattering term containing two collisions gives a negative contribution to  $\sigma_{tot}$ .

Let us now consider the contribution to  $d\sigma/dy$ . It is given by  $\sigma_2^1(b) + 2\sigma_2^2(b) = 0$ . Indeed, in the case of a double inelastic collision, the triggered particle can be emitted in either of them – hence an extra factor 2. This is just the AGK cancellation. It is easy to see that it is valid order by order in the total number of collisions. This can also be seen as follows. The total inelastic cross-section for  $pA$  collision in the Glauber model is given by the well known expression

$$\sigma_{inel}^{pA}(b) = \sum_{n=1}^A \sigma_n(b) = 1 - (1 - \sigma_{inel} T_A(b))^A . \quad (\text{A.2})$$

This expression contains a term in  $A^1$  (Born term or impulse approximation). It also contains contribution from multiple scattering with alternate signs. Numerically, it behaves as  $A^\alpha$  with  $\alpha \sim 2/3$ . The single particle inclusive cross-section is given by

$$\frac{d\sigma^{pA}}{dy}(b) \propto \sum_{n=1}^A n \sigma_n(b) = A \sigma_{inel} T_A(b) . \quad (\text{A.3})$$

We see that here multiple-scattering contributions cancel identically and only the Born term is left. As a consequence of this AGK cancellation the  $A$ -dependence of  $d\sigma/dy$  in  $pA$  interactions behaves as  $A^1$ . In the case

of  $AB$  collisions it behaves as  $AB$  and  $dN^{AB}/dy = (1/\sigma_{AB})d\sigma^{AB}/dy$  is proportional to the number of binary collisions – rather than to the number of participants.

We see in this way that the AGK rules are trivially satisfied in the Glauber model. As mentioned in Section A.1 in the Glauber model only the initial state is present in the vertex function (blob). Thus a secondary can only be produced in an interaction and the AGK cancellation is exact. In a general theory with a more complicated vertex function, the triggered particle may be produced in the blob. As discussed in Section A.2 this gives rise to a violation of the AGK cancellation – which is responsible for the shadowing corrections to the inclusive spectra.

## Appendix B

In order to get the relative densities of each baryon and antibaryon species we use simple quark counting rules [6] [31]. Denoting the strangeness suppression factor by  $S/L$  (with  $2L + S = 1$ ), baryons produced out of three sea quarks (which is the case for pair production) are given the relative weights

$$I_3 = 4L^3 : 4L^3 : 12L^2S : 3LS^2 : 3LS^2 : S^3 \quad (\text{B.1})$$

for  $p$ ,  $n$ ,  $\Lambda + \Sigma$ ,  $\Xi^0$ ,  $\Xi^-$  and  $\Omega$ , respectively. The various coefficients of  $I_3$  are obtained from the power expansion of  $(2L + S)^3$ .

For net baryon production, we have seen in Section 5 that the baryon can contain either one or two sea quarks. The first case corresponds to direct diquark fragmentation described by the second term of Eq. (12). The second case corresponds to diquark splitting, described by the first term of (12). In these two cases, the relative densities of each baryon species are respectively given by

$$I_1 = L : L : S \quad (\text{B.2})$$

for  $p$ ,  $n$  and  $\Lambda + \Sigma$ , and

$$I_2 = 2L^2 : 2L^2 : 4LS : \frac{1}{2}S^2 : \frac{1}{2}S^2 \quad (\text{B.3})$$

for  $p$ ,  $n$ ,  $\Lambda + \Sigma$ ,  $\Xi^0$  and  $\Xi^-$ . The various coefficients in (B.2) and (B.3) are obtained from the power expansion of  $(2L + S)$  and  $(2L + S)^2$ , respectively.

In order to take into account the decay of  $\Sigma^*(1385)$  into  $\Lambda\pi$ , we redefine the relative rate of  $\Lambda$ 's and  $\Sigma$ 's using the empirical rule  $\Lambda = 0.6(\Sigma^+ + \Sigma^-)$

– keeping, of course, the total yield of  $\Lambda$ 's plus  $\Sigma$ 's unchanged. In this way the normalization constants of all baryon species in pair production are determined from one of them. This constant, together with the relative normalization of  $K$  and  $\pi$ , are determined from the data for very peripheral collisions. In the calculations we use  $S = 0.1$  ( $S/L = 0.22$ ).

## REFERENCES

- [1] A. Capella, *Acta Physica Polonica B* **30** (1999) 3541.
- [2] A. Capella and D. Sousa, *Phys. Lett. B* **511** (2001) 185.
- [3] D. Kharzeev and M. Nardi, *Phys. Lett. B* **507** (2001) 121.  
D. Kharzeev and E. Levin, *Phys. Lett. B* **523** (2001) 79.
- [4] J. Schaffner-Bielich, D. Kharzeev, L. McLerran and R. Venugopalan, *Nucl. Phys. A* **705** (2002) 494.
- [5] A. Capella, *Phys. Lett. B* **542** (2002) 63.
- [6] A. Capella, C. A. Salgado and D. Sousa, *nucl-th/0205014*.
- [7] A. Capella, A. Kaidalov and D. Sousa, *Phys. Rev. C* **65** (2002) 054908.
- [8] A. Capella and D. Sousa, *nucl-th/0110072*.
- [9] A. Capella, U. Sukhatme, C-I Tan and J. Tran Thanh Van, *Phys. Rep.* **236** (1994) 225.
- [10] A. Kaidalov, in : L. Ciafarelli and Yu Dokshitzer eds, *QCD at 200 TeV* (Plenum Press, New York), p. 1 (1992).
- [11] G. t'Hooft, *Nucl. Phys. B* **72** (1974) 461.
- [12] G. Veneziano, *Nucl. Phys. B* **74** (1974) 365.
- [13] G. Veneziano, *Nucl. Phys. B* **117** (1976) 519.
- [14] V. N. Gribov, *ZhETF* **57** (1967) 654.
- [15] M. Ciafaloni, G. Marchesini and G. Veneziano, *Nucl. Phys. B* **98** (1975) 472.
- [16] A. Capella, *Acta Phys. Polonica B* **15** (1984) 1185.
- [17] A. Capella, J. Kwiecinski and J. Tran Thanh Van, *Phys. Lett. 108B* (1982) 347.  
A. Capella, C. Pajares and A. Ramallo, *Nucl. Phys. B* **241** (1984) 175.
- [18] A. Capella, A. Kaidalov and J. Tran Thanh Van, *Heavy Ion Physics* **9** (1999).
- [19] A. Schwimmer, *Nucl. Phys. B* **94** (1975) 445.
- [20] O. Kancheli, *JETP* **18** (1973) 465.
- [21] PHOBOS collaboration, B. B. Back et al, *nucl-ex/0302015*.  
STAR collaboration, C. Adler et al, *nucl-ex/0206011*.
- [22] PHENIX collaboration, S. Mioduszeski, *nucl-ex/0210021*.
- [23] B. Z. Kopeliovich, J. Nemchik, A. Schäfer and A. V. Tarasov, *hep-ph/0201010*.
- [24] D. Kharzeev, E. Levin and L. McLerran, *hep-ph/0210332*.

- [25] NA 49 collaboration, H. Appelshäuser et al, Phys. Rev. Lett. **82** (1999) 2471.
- [26] G. C. Rossi and G. Veneziano, Nucl. Phys. **123** (1977) 507.
- [27] B. Z. Kopeliovich and B. G. Zakharov, Sov. J. Nucl. Phys. **48** (1988) 136 ; Z. Phys. C **43** (1989) 241.
- [28] G. H. Arakelyan, A. Capella, A. B. Kaidalov and Yu. M. Shabelski, Eur. Phys. J. C **26** (2002) 81.
- [29] D. Kharzeev, Phys. Lett. B **378** (1996) 238.
- [30] A. Capella and B. Z. Kopeliovich, Phys. Lett. B **381** (1996) 325.
- [31] A. Capella and C. A. Salgado, New Journal of Phys. **2** (2000) 30.1 ; Phys. Rev. C **60** (1999) 054906.  
A. Capella, E. G. Ferreiro and C. A. Salgado, Phys. Lett. **81B** (1979) 68.
- [32] B. Koch, U. Heinz and J. Pitsut, Phys. Lett. **B243** (1990) 149.
- [33] PHENIX collaboration, K. Adcox et al., nucl-ex/0112006.
- [34] STAR collaboration, C. Adler et al., Phys. Rev. Lett. **87** (2001) 262302.
- [35] STAR collaboration, J. Castillo, Proceedings Quark Matter 2002 (Nantes, France).
- [36] STAR collaboration, C. Adler et al., Phys. Rev. Lett. **86** (2001) 4778.
- [37] J. Ranft, A. Capella and J. Tran Thanh Van, Phys. Lett. B **320** (1999) 346.  
N. S. Amelin, N. Armesto, C. Pajares and D. Sousa, Eur. Phys. J. **C222** (2001) 149.
- [38] P. Cortese, NA50 collaboration, Proceedings Quark Matter 2002, Nantes, France.
- [39] J. L. Ramello, NA50 collaboration, Proceedings Quark Matter 2002, ibid.
- [40] A. Capella, E. G. Ferreiro and A. Kaidalov, Phys. Rev. Lett. **85** (2000) 2080.
- [41] N. Armesto and A. Capella, Phys. Lett. **B 393** (1998) 431.
- [42] A. Capella and D. Sousa, in preparation.
- [43] N. Armesto, A. Capella and E. G. Ferreiro, Phys. Rev. **C59** (1999) 345.  
A. K. Chaudhuri, nucl-th/0212046.
- [44] NA57 collaboration, N. Carrer, Nucl. Phys. **A698** (2002) 118c.
- [45] A. Capella, J. Kwiecinski and J. Tran Thanh Van, Phys. Rev. Lett. **58** (1987) 2015.
- [46] V. Abramovski, V. N. Gribov and O. Kancheli, Sov. J. Nucl. Phys. **18** (1974) 308.

**Table 1**

Calculated values [5] of the rapidity distribution of  $pp \rightarrow p - \bar{p} + X$  at  $\sqrt{s} = 17.2$  GeV and 27.4 GeV ( $k = 1.4$ ) and  $\sqrt{s} = 130$  GeV ( $k = 2$ ). (In order to convert  $d\sigma/dy$  into  $dN/dy$  a value of  $\sigma = 30$  mb has been used). For comparison with the nucleus-nucleus results, all values in this table have been scaled by  $n_A = 175$  – the number of participant pairs in central  $Pb$   $Pb$  and  $Au$   $Au$  collisions. Data are in brackets.

$y^*$	$pp \rightarrow p - \bar{p}$	$pp \rightarrow p - \bar{p}$	$pp \rightarrow p - \bar{p}$
	$\sqrt{s} = 17.2$ GeV	$\sqrt{s} = 27.4$ GeV	$\sqrt{s} = 130$ GeV
0	9.2	6.5	3.6
		[6.3 $\pm$ 0.9]	
1	15.0	9.3	4.2
	[16.1 $\pm$ 1.8]	[9.6 $\pm$ 0.9]	
1.5	25.8	14.6	5.1
	[24.1 $\pm$ 1.4]	[15.4 $\pm$ 0.9]	
2	47.1	26.2	6.8
	[45.4 $\pm$ 1.4]	[27.7 $\pm$ 0.9]	

**Table 2**

Calculated values [5] of the rapidity distribution  $dN/dy$  for central  $Pb$   $Pb \rightarrow p - \bar{p} + X$  and  $Pb$   $Pb \rightarrow B - \bar{B} + X$  at  $\sqrt{s} = 17.2$  GeV ( $k = 1.4$ ) and central  $Au$   $Au \rightarrow p - \bar{p} + X$  and  $Au$   $Au \rightarrow B - \bar{B} + X$  at  $\sqrt{s} = 130$  GeV ( $k = 2$ ) and  $\sqrt{s} = 200$  GeV ( $k = 2.2$ ) . The centrality has been defined by the number of participant pairs ( $n_A = 175$  at all energies) and  $\nu = n/n_A = 4.5$ , 5.0 and 5.2 at  $\sqrt{s} = 17.2$ , 130 and 200 GeV, respectively. Data are in brackets.

$y^*$	$Pb$ $Pb \rightarrow p - \bar{p}$	$Pb$ $Pb \rightarrow B - \bar{B}$	$Au$ $Au \rightarrow p - \bar{p}$	$Au$ $Au \rightarrow B - \bar{B}$
	$\sqrt{s} = 17.2$ GeV	$\sqrt{s} = 17.2$ GeV	$\sqrt{s} = 130$ (200) GeV	$\sqrt{s} = 130$ (200 GeV)
0	23.0	58.5	8.0 (7.4)	20.9 (18.9)
	[26.7 $\pm$ 3.7]	[67.7 $\pm$ 7.3]	[5.6 $\pm$ 0.9 $\pm$ 24%]	
1	32.3	79.7	9.7 (8.7)	22.6 (22.0)
	[34.9 $\pm$ 1.5]	[84.7 $\pm$ 3.5]		
1.5	36.3	87.0	12.3 (10.9)	31.5 (27.4)
	[34.4 $\pm$ 1.7]	[80.0 $\pm$ 3.9]		
2	25.3	57.15	17.3 (14.3)	43.4 (35.9)
	[24.7 $\pm$ 1.5]	[56.1 $\pm$ 3.1]		

### Figure captions

**Figure 1** : The mechanism of particle production in  $e^+e^-$  annihilation. The net of soft gluons and quark loops is only shown here and in Fig. 6.

**Figure 2** : One string diagram in  $\bar{p}p$ .

**Figure 3** : Dominant two-chain (single cut Pomeron) contributions to high energy  $\pi^+$ -proton collisions.

**Figure 4** : Dominant two-chain contribution to proton-antiproton collisions at high energies (single cut Pomeron).

**Figure 5** : Dominant two-chain diagram describing multiparticle production in high energy proton-proton collisions (single cut Pomeron).

**Figure 6** : Single Pomeron exchange and its underlying cylindrical topology. This is the dominant contribution to proton-proton elastic scattering at high energies.

**Figure 7** : Two cut Pomeron (four-chain) diagram for proton-proton collisions.

**Figure 8** : The values of  $dN^{ch}/dy$  per participant for  $Pb\ Pb$  collisions at  $\sqrt{s} = 17.3$  GeV computed [2] from eq. (2), compared with WA98 data.

**Figure 9** : The values of  $dN^{ch}/d\eta_{c.m.}/(0.5\ n_{part})$  for  $Au\ Au$  collisions at  $\sqrt{s} = 130$  GeV computed [2] from eq. (2) including shadowing corrections are given by the dark band in between solid lines. The PHENIX data are also shown (black circles and shaded area).

**Figure 10** : (a) Calculated values [6] of  $dN/dy$  of  $p$  (solid line)  $\bar{p}$  (dashed line), and  $p - \bar{p}$  (dotted line) at mid rapidities,  $|y^*| < 0.35$ , are plotted as a function of  $dN_{h^-}/d\eta$ , and compared with PHENIX data [33] ; (b) same for  $\Lambda$  and  $\bar{\Lambda}$  compared with preliminary STAR data [34] ; (c) same for  $\Xi^-$  and  $\bar{\Xi}^+$  compared to preliminary STAR data [35] ; (d) same for  $\Omega$  and  $\bar{\Omega}$ .

**Figure 11** : Calculated values [6] of the ratios  $B/n_{part}$  (a) and  $\bar{B}/n_{part}$  (b), normalized to the same ratio for peripheral collisions ( $n_{part} = 18$ ), plotted as a function of  $n_{part}$ .

**Figure 12 :** The ratio of  $J/\psi$  over  $DY$  cross-sections in  $Pb$   $Pb$  collisions at 158 GeV/c versus  $E_T$  obtained [42] in the comovers interaction model with  $\sigma_{abs} = 4.5$  mb and  $\sigma_{co} = 0.65$  mb. The absolute normalization is 47. The preliminary data are from [39].

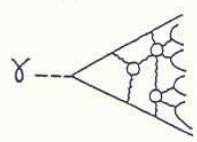


Figure 1

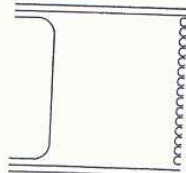


Figure 2

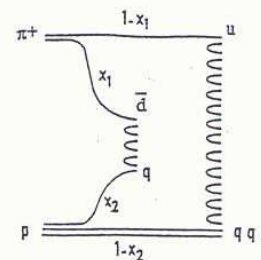


Figure 3

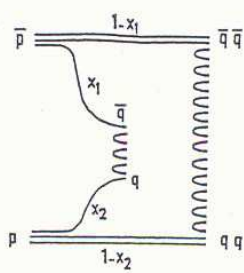


Figure 4

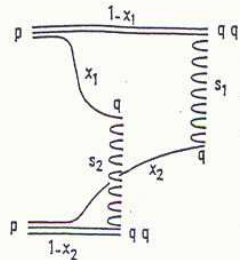


Figure 5

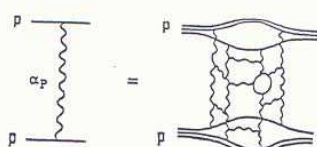


Figure 6

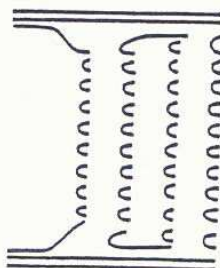


Figure 7

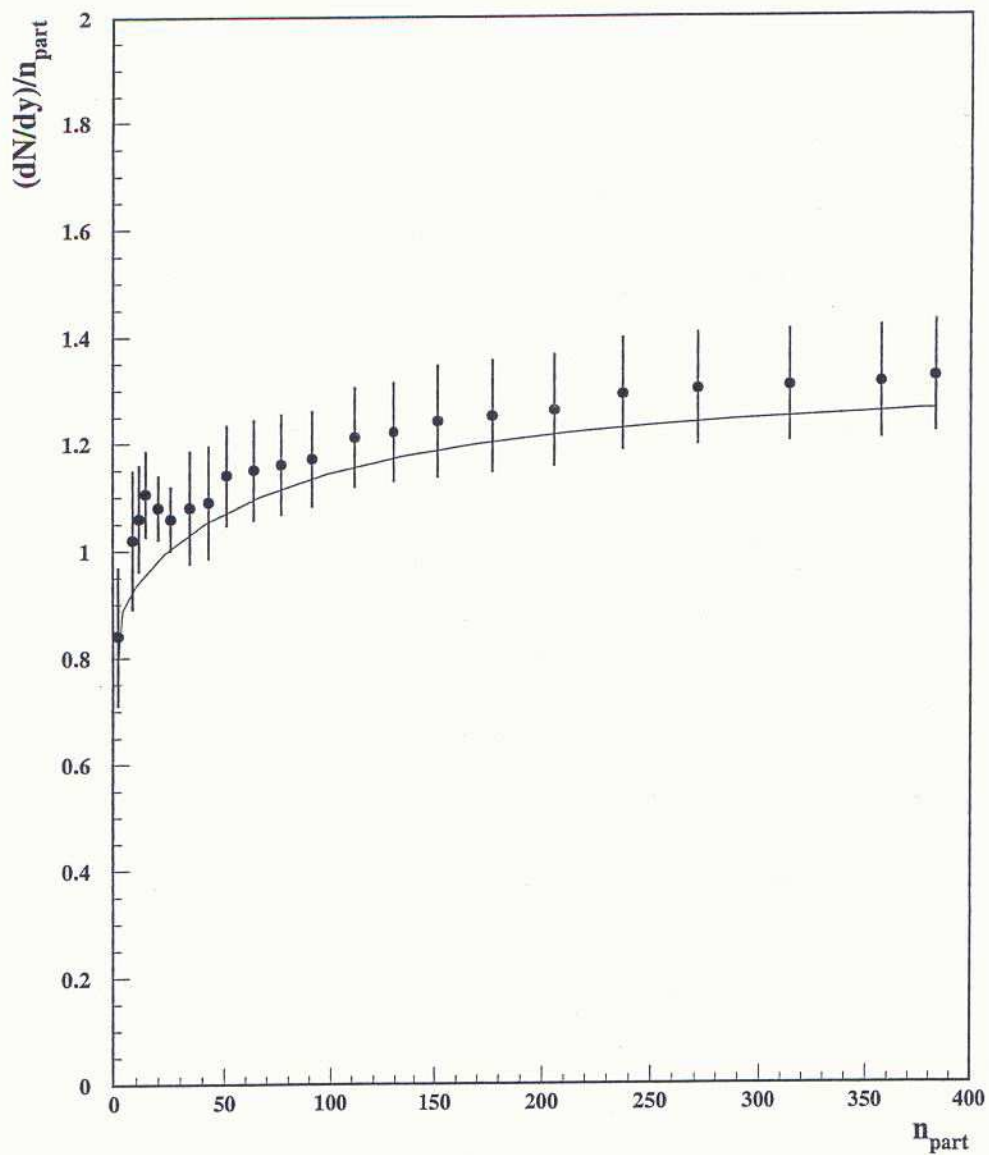


Figure 8

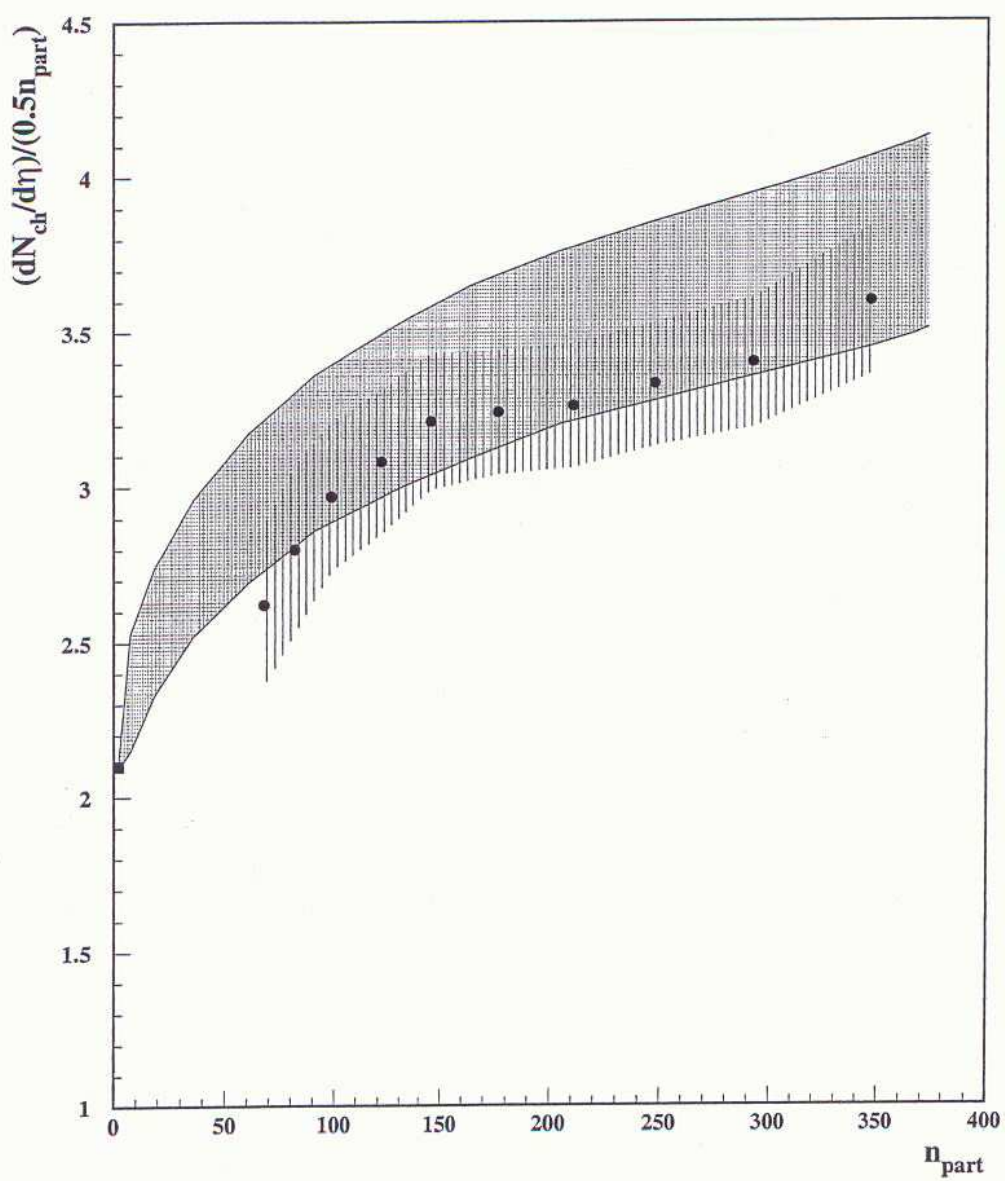


Figure 9

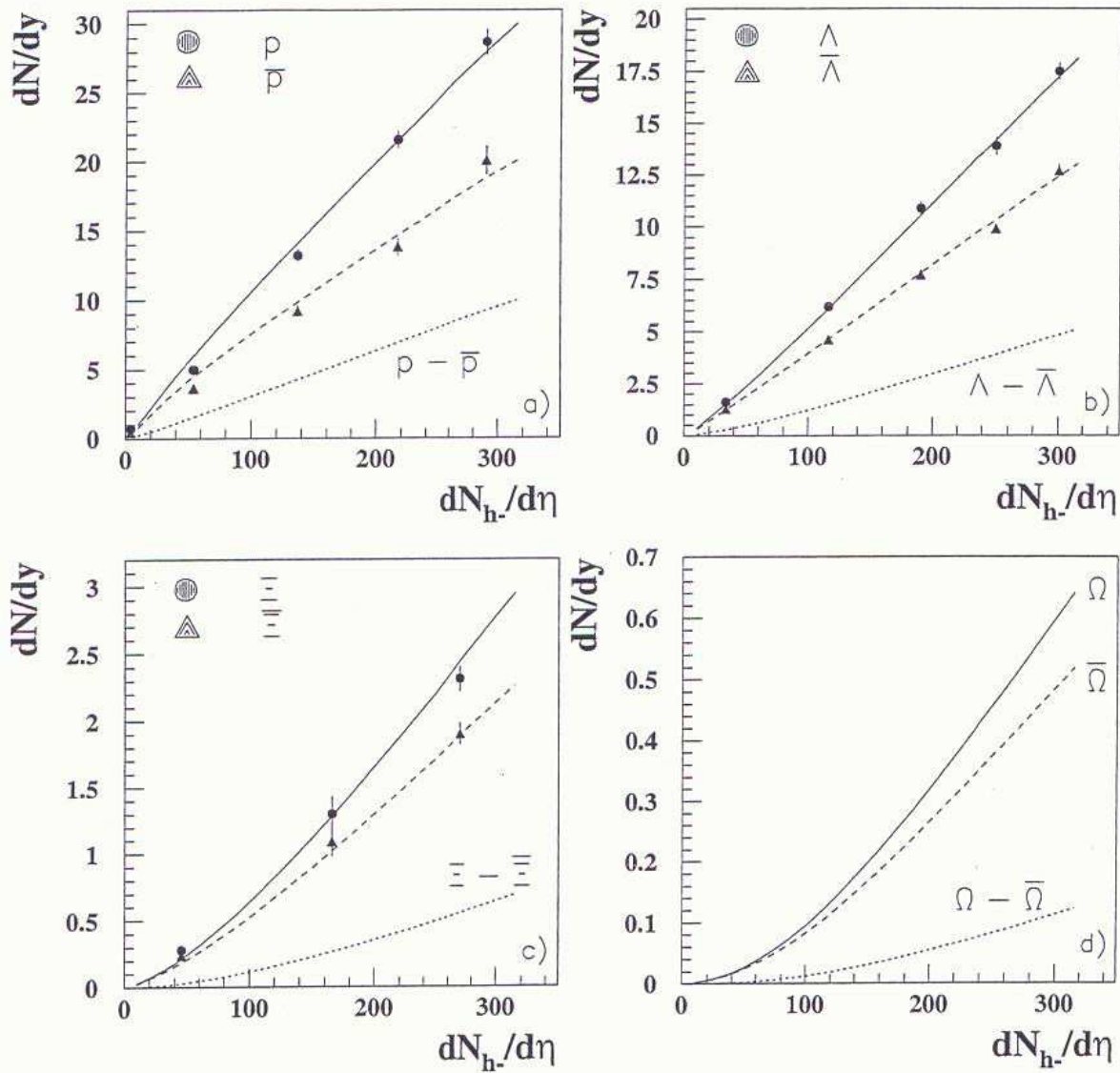


Figure 10

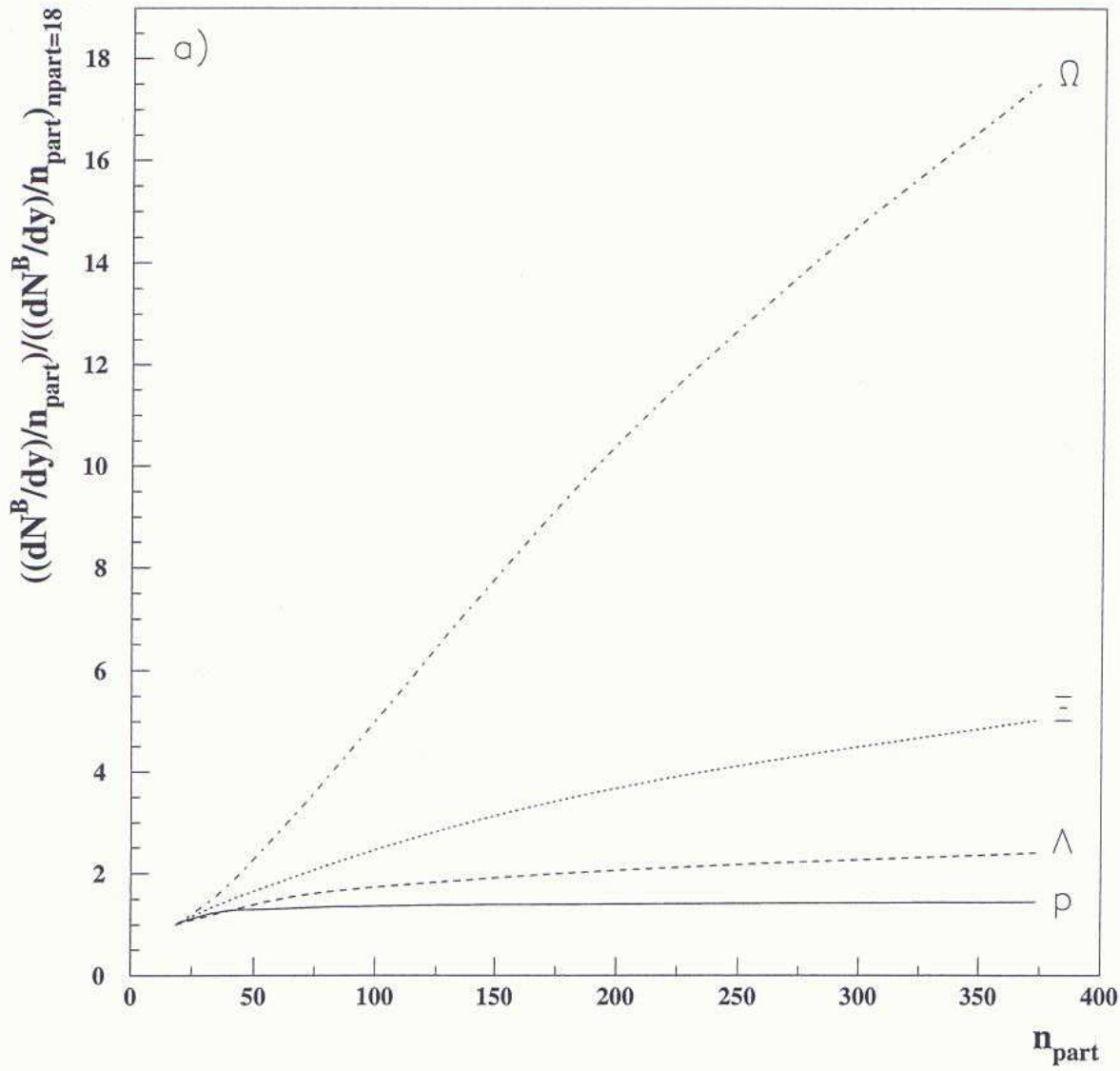


Figure 11a

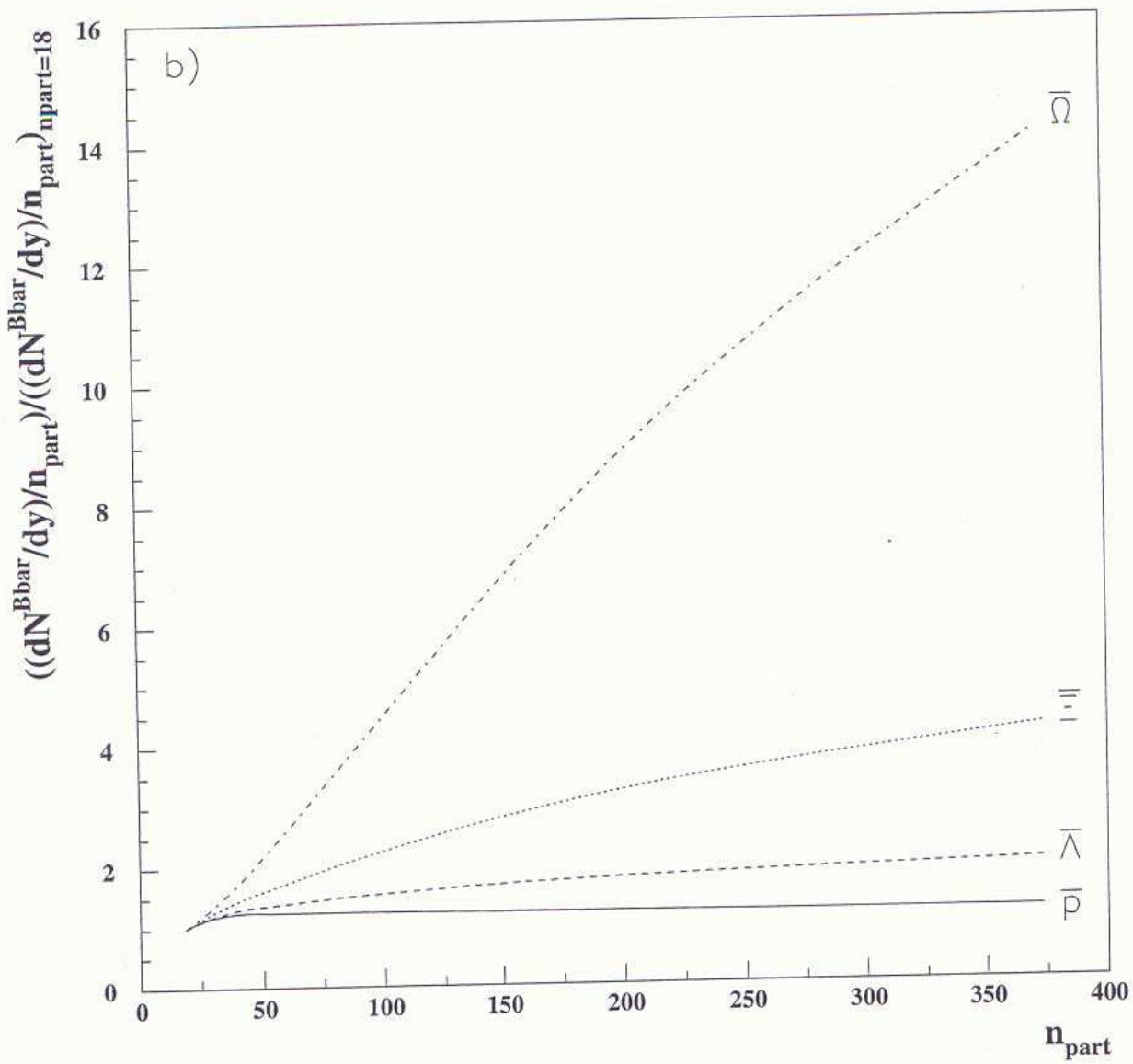


Figure 11b

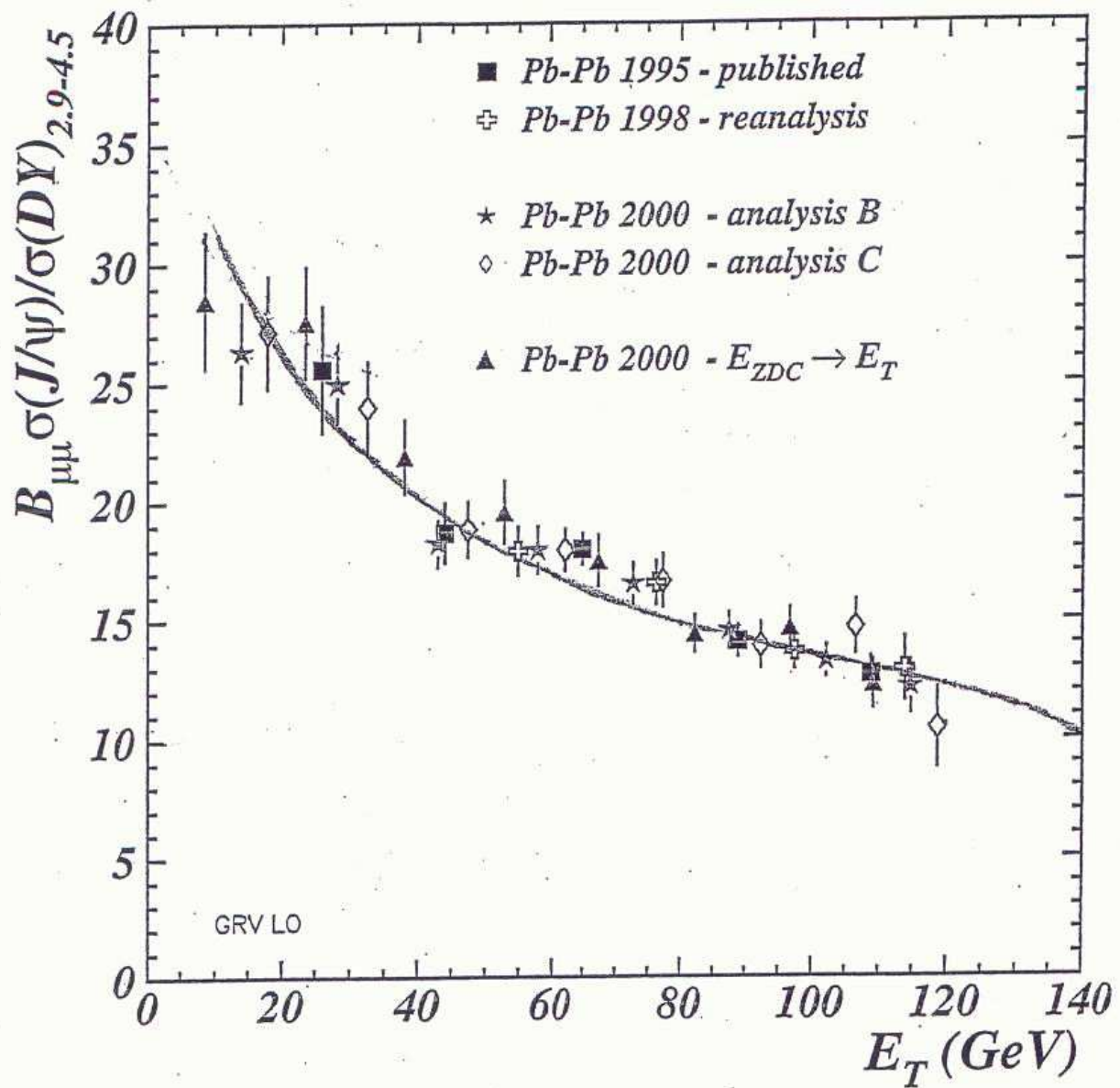


Figure 12